



Symmetric and asymmetric components of anomalous tropospheric-mean horizontal fluxes of latent and sensible heat associated with ENSO events of variable magnitude



Evan Kutta^{a,*}, Jason A. Hubbart^b, Bohumil M. Svoma^c, Timothy Eichler^d, Anthony R. Lupo^e

^a University of Missouri, School of Natural Resources, Department of Atmospheric Sciences, 203-T ABNR Building, Columbia, MO 65201, USA

^b West Virginia University, Institute of Water Security and Science, Davis College, Schools of Agriculture and Food, and Natural Resources, 3107 Agricultural Sciences Building, Morgantown 26506, WV, USA

^c University of Missouri, School of Natural Resources, Department of Atmospheric Sciences, 302-A ABNR Building, Columbia, MO 65201, USA

^d Saint Louis University, School of Education, Fitzgerald Hall 016, Saint Louis, MO 63103, USA

^e University of Missouri, School of Natural Resources, Department of Atmospheric Sciences, 302-E ABNR Building, Columbia, MO 65201, USA

ARTICLE INFO

Keywords:

ENSO phenomena
Symmetry of tropospheric response
Pacific North American pattern
North Atlantic Oscillation
Climate change
Teleconnections

ABSTRACT

The El Niño–Southern Oscillation (ENSO) represents the dominant mode of global climate variability and is inherently nonlinear such that the linearity of the atmospheric response remains an area of ongoing research. The phase of North Atlantic Oscillation (NAO) and Pacific North American (PNA) patterns of intra-annual climate variability are favored to be the same as the phase of ENSO resulting in important climate impacts across Europe and North America. Advanced understanding of the symmetry of this response at global scale using monthly composite analyses of anomalous horizontal sensible and latent heat fluxes at various ENSO event magnitudes quantified from ERA-Interim output (January 1979 through June 2016) will advance impact predictability. A linear relationship between ENSO, PNA, and NAO patterns was identified, particularly for strong ENSO events. The nonlinear component indicated general eastward (westward) shifts in anomalous heat fluxes during El Niño (La Niña) events such that the greatest impacts were implied across North America during Decembers and Januarys of strong El Niño and weak La Niña events. Analyses of anomalous latent heat fluxes indicated spatial patterns consistent with more frequent atmospheric river phenomena, especially during Decembers and Januarys of strong El Niño events. This work demonstrates that the symmetric component of anomalous horizontal, tropospheric-mean heat fluxes corresponding to ENSO events are effective for identifying north-south dipoles of anomalous circulations consistent with PNA or NAO patterns and connections between tropical heat source regions and the PNA and NAO regions. This work also demonstrates the asymmetric component identified differences in anomalous circulation position and whether El Niño or La Niña resulted in larger heat flux anomalies. Therefore, this work provides insight into impacts associated with future ENSO events, especially across North America during strong El Niño and weak La Niña.

1. Introduction

On inter-annual time scales, the El Niño–Southern Oscillation (ENSO) represents the most important coupled ocean–atmosphere climate phenomena (Wolter and Timlin, 2011). ENSO is characterized by an oscillation of sea surface temperature (SST) anomalies within the tropical Pacific Ocean, most commonly the Niño 3.4 region (5°N–5°S, 170°W–120°W; Harrison and Chiodi, 2017). Tropical SST anomalies

were previously shown to influence surface fluxes of moisture, heat, and momentum that adjusted the tropical atmospheric circulation forcing large-scale atmospheric Rossby waves in preferred locations that propagated into extratropical latitudes (Trenberth et al., 1998). Thus, anomalous tropospheric heating associated with ENSO forces extratropical impacts through what is commonly referred to as the atmospheric bridge phenomena (e.g. Alexander et al., 2002; Lau and Nath, 1996). The atmospheric bridge refers to the atmosphere's ability to link

Abbreviations: ENSO, El Niño–Southern Oscillation; SST, Sea surface temperature; NAO, North Atlantic Oscillation; PNA, Pacific North American pattern; NSD, North–South dipole; ERA-I, ERA-Interim Project; NDJ, November, December, January; CPC, Climate Prediction Center; ONI, Oceanic Niño Index; ASHF, anomalous sensible heat flux; ALHF, anomalous latent heat flux; EWD, east–west circulation dipole; US, United States

* Corresponding author.

E-mail addresses: ejk3md@mail.missouri.edu (E. Kutta), Jason.Hubbart@mail.wvu.edu (J.A. Hubbart), svomab@missouri.edu (B.M. Svoma), teichler@slu.edu (T. Eichler), LupoA@missouri.edu (A.R. Lupo).

<http://dx.doi.org/10.1016/j.atmosres.2017.08.013>

Received 7 April 2017; Received in revised form 19 July 2017; Accepted 12 August 2017

Available online 14 August 2017

0169-8095/ © 2017 Elsevier B.V. All rights reserved.

two distant regions of anomalous sea surface temperatures through fluxes of energy, mass, and momentum (Lau and Nath, 1996). Mechanistically, atmospheric bridging can be thought of as anomalous poleward heat fluxes associated with ENSO's tropical heating patterns. These horizontal heat fluxes are necessary to maintain climate equilibrium (e.g. Trenberth and Stepaniak, 2003). Therefore, spatial distribution of anomalous horizontal heat fluxes during ENSO events is of considerable interest given that ENSO disturbs the horizontal atmospheric circulation through anomalous vertical heat fluxes into the tropical atmosphere. The resulting cascade of extratropical climate impacts projects onto multiple patterns of climate variability (Liu and Alexander, 2007).

ENSO's primary extratropical effect is to alter the predictability of mid-latitude climate phenomena such as the North Atlantic Oscillation (NAO) and Pacific North American (PNA) patterns (e.g. Hurrell and Deser, 2010; Straus and Shukla, 2002). The NAO and PNA patterns originate from mid-latitude dynamics separate from the ENSO phenomena (e.g. Hurrell and Deser, 2010; Straus and Shukla, 2002) and each represent dominant patterns of Northern Hemisphere mid-latitude climate variability (e.g. Franzke et al., 2011; Hurrell and Deser, 2010). Straus and Shukla (2002) explicated that the presence of ENSO forcing skewed the probability density function of positive or negative phases of the PNA pattern such that a linear relationship between ENSO and PNA patterns is commonly observed. A similar, climatologically relevant, link between ENSO and NAO patterns of climate variability has also been proposed by Brönnimann (2007). Hurrell and Deser (2010) described NAO and PNA patterns as north-south dipoles (NSDs) characterized by simultaneously out of phase height anomalies between temperate and high latitude regions. The NAO pattern has a single NSD located over the North Atlantic Ocean and the PNA pattern has a pair of simultaneously out of phase NSDs across the northeastern Pacific Ocean and North America. Representative locations (one-point correlations) for PNA (45°N 165°W) and NAO (65°N 30°W) patterns (Hurrell and Deser, 2010) were located east of the climatologic position of the Aleutian (52°N 175°E; Serreze et al., 1997) and Icelandic low pressure systems (62°N 35°W; Rodionov et al., 2007). Both NAO (e.g. Rodwell et al., 1999) and PNA (Leathers et al., 1991; Leathers and Palecki, 1992) patterns have regional climate impacts including precipitation (Seager et al., 2010) and temperature (Fu and Yao, 2015) anomalies across Europe and North America, respectively. Given the important climate impacts associated with each pattern there is a need to better understand the spatial and temporal variability of the influence ENSO forcing has on PNA and NAO patterns.

Both ENSO forcing and the subsequent atmospheric response have been shown to have symmetric and asymmetric components of similar magnitude such that each produced climatologically relevant extratropical impacts (Zhang et al., 2014). The simultaneous existence of both large symmetric and asymmetric components suggests that traditional linear techniques (e.g. regression or empirical orthogonal function analyses) are insufficient to reveal all climatologically relevant impacts associated with the ENSO phenomena (Okumura and Deser, 2010). Furthermore, SST anomalies associated with the ENSO phenomena have been characterized by their asymmetric magnitude (e.g. An and Jin, 2004) and duration (Okumura and Deser, 2010) resulting in symmetric and asymmetric atmospheric responses that are of the same order of magnitude (e.g. Zhang et al., 2014). The most common way to analyze the symmetric and asymmetric atmospheric responses to ENSO forcing is through composite analyses of 500 mb height, surface temperature, and precipitation anomalies (Zhang et al., 2014). However, using atmospheric reanalysis output to directly quantify anomalous horizontal fluxes of sensible and latent heat advances mechanistic understanding of how atmospheric and oceanic media transport heat poleward to maintain climate equilibrium (Kim and Alexander, 2015). Use of state-of-the-art atmospheric reanalysis output is critical to advance understanding of a suite of hydrometeorological research topics including the atmospheric response to ENSO forcing (Lorenz and

Kunstmann, 2012). Large quantities of historic observations from various observation platforms were processed using advanced data assimilation techniques (e.g. 4D-Var; Dee et al., 2011) to provide spatiotemporally continuous, gridded atmospheric reanalyses over a long period of record (1979–present). Quantifying symmetric and asymmetric components of anomalous atmospheric heat fluxes using atmospheric reanalysis output will clarify spatial patterns of the atmospheric bridge phenomena to better understand the cascade extratropical climate impacts (ENSO; Alexander et al., 2002).

This cascade of extratropical impacts is driven by anomalous upward heat flux from the Pacific Ocean into the troposphere (Peixoto and Oort, 1992). However, a limited number of studies examining anomalous tropospheric-mean fluxes of sensible or latent heat associated with ENSO exist and neither the seasonal evolution nor its symmetry have been assessed at the global scale. Therefore, the overarching objective of this work was to use the ERA-Interim atmospheric reanalysis project (ERA-I; Dee et al., 2011) data output to quantify symmetric and asymmetric components of the atmospheric response to ENSO forcing through horizontal, tropospheric-mean analyses of latent and sensible heat flux anomalies. Sub-objectives included, a) assess symmetry of anomalous fluxes of sensible and latent heat and whether spatial patterns in anomalous fluxes are consistent with PNA and NAO teleconnections, b) assess spatially continuous connections between tropical heat sources and PNA and NAO regions c) assess the influence of ENSO forcing magnitude on the magnitude and symmetry of the atmospheric response. Quantifying anomalous fluxes of tropospheric heat will identify the favored phase of either PNA or NAO patterns during November, December, January (NDJ) months associated with ENSO events of various magnitudes. This work advances understanding of the interrelationship between ENSO, PNA, and NAO patterns and the connection to tropical heat sources, which could enhance predictability of climate impacts, including atmospheric river events, across North America and Western Europe.

2. Materials and methods

2.1. Identifying ENSO events

Each El Niño and La Niña event occurring since 1950 has been documented by the Climate Prediction Center (CPC; Kirtman et al., 2014) using the Oceanic Niño Index (ONI; Yu and Kim, 2013). The ONI is quantified by calculating SST anomalies within the Niño 3.4 region (170°W to 120°W, 5°S to 5°N) averaged over three consecutive monthly periods. Harrison and Chiodi (2017) described the current operational definition of an El Niño (La Niña) event as five or more consecutive ONI values greater (less) than or equal to 0.5 °C (−0.5 °C). Using this definition, thirteen El Niño and nine La Niña events were identified over the period of record for the current work (January 1979 through June 2016). However, asymmetries in the SST anomaly magnitude (e.g. An and Jin, 2004) and duration are associated with ENSO events such that La Niña events are characterized by smaller SST anomalies that persist for a longer period of time (e.g. Okumura and Deser, 2010). This asymmetry suggests that criteria for La Niña events should be reduced to have a more equal number of El Niño and La Niña events consistent with an oscillation (El Niño-Southern Oscillation). Reducing the persistence of negative SST anomalies from five to four consecutive ONI values (tri-monthly averages) identified three additional La Niña events such that samples sizes of El Niño (13) and La Niña (12) events were consistent with an oscillation from one phase to the other. All El Niño and La Niña events that occurred during the period of record were summarized in Table 1. The January 1979 through June 2016 period of record was chosen given temporal limitations of ERA-I and because June 2016 represented the end of the strong 2015–2016 El Niño event.

The atmospheric response to ENSO forcing will be quantified using output from the composited during ENSO events occurring between January 1979 and June 2016. Composite analyses are a common

Table 1

Summary of all thirteen El Niño events and twelve La Niña events occurring between 1979 and 2016 including maximum and minimum ONI values, each tri-monthly period when maximum or minimum ONI values occurred, and categorization of each ENSO event.

El Niño events			La Niña events		
Years	Max ONI	Category	Years	Min ONI	Category
1979–80	0.6	Weak	1983–84	−0.8	Weak
1982–83	2.1	Strong	1984–85	−1.1	Moderate
1986–87	1.2	Moderate	1988–89	−1.8	Strong
1987–88	1.6	Moderate	1995–96	−1.0	Moderate
1991–92	1.6	Moderate	1998–99	−1.4	Moderate
1994–95	1.0	Moderate	1999–00	−1.6	Strong
1997–98	2.3	Strong	2000–01	−0.8	Moderate
2002–03	1.2	Moderate	2005–06	−0.7	Weak
2004–05	0.7	Weak	2007–08	−1.4	Moderate
2006–07	0.9	Moderate	2008–09	−0.7	Weak
2009–10	1.3	Moderate	2010–11	−1.5	Strong
2014–15	0.6	Weak	2011–12	−1.0	Moderate
2015–16	2.3	Strong			

Max ONI = Maximum Oceanic Niño Index, Min ONI = Minimum Oceanic Niño Index.

method for showing atmospheric anomalies associated with ENSO forcing of variable magnitudes (e.g. Müller and Roeckner, 2008) and season (e.g. Fogt and Bromwich, 2006). Therefore, each ENSO event was categorized into weak, moderate, or strong categories based on the magnitude of maximum or minimum SST anomalies (Table 1). Weak ENSO events were identified as the three smallest maximum (minimum) SST anomalies, strong ENSO events were identified as the three largest maximum (minimum) SST anomalies, and remaining ENSO events were categorized as moderate El Niño (La Niña) events. Results will be focused on composite analyses of all 25 ENSO events, six strong ENSO events, and six weak ENSO events. Results of the 13 moderate ENSO events were not shown in this work since they were not substantially different from the composite of all 25 ENSO events. Composites of six strong and weak ENSO events provide a realistic range of influence ENSO events had on tropospheric circulations. Additionally, maximum ONI indices were clustered near the operational definition (0.6, 0.7, 0.6, −0.8, −0.7, −0.7) for weak ENSO events and at approximately four times the operational definition (2.1, 2.3, 2.3, −1.8, −1.6, −1.5) for strong ENSO events (Table 1). The most common occurrence of maximum or minimum tri-monthly mean SST forcing associated with ENSO events during this period of record was the November, December, January (NDJ) period. Nine of the thirteen El Niño events and eight of the twelve La Niña events peaked during NDJ and SSTA variance is also maximized during December (Okumura and Deser, 2010). For these reasons NDJ was treated as the tri-monthly period analyzed in this work. All analyses will be performed at the global scale as recommended by Trenberth and Caron (2000), but results and discussion will be focused on the atmospheric response across the northern Pacific and Atlantic Oceans.

2.2. Reanalysis data used

The ERA-I data set was produced at high spatial ($\sim 0.7^\circ$ lat/lon) and temporal (6-hourly analyses) resolution over a global domain by the European Centre for Medium-Range Weather Forecasts (Dee et al., 2011). ERA-I and NCEP-NCAR (National Centers for Environmental Prediction-National Center for Atmospheric Research) atmospheric reanalyses are the most often used reanalysis products and both reproduced observed spatial patterns of temperature and precipitation well (Fu et al., 2016). Estimates of temperature and specific humidity from ERA-I were comparatively better than the NCEP-NCAR reanalyses (Fu et al., 2016), which is why ERA-I output was selected for this work. However, Lorenz and Kunstmann (2012) cautioned against the use of ERA-I for climate trend analyses and long-term water budget studies,

which are beyond the scope of this work. The subset of ERA-I output utilized for the current work included six-hourly model analyses of specific humidity (q), temperature (T), and zonal (u) and meridional (v) components of wind to allow for direct calculation of horizontal fluxes of sensible and latent heat. Data was acquired on original model levels that were defined using an eta vertical coordinate system characterized by pressure coordinates in the upper atmosphere, hybrid pressure-sigma coordinates at mid to low levels, and terrain-following sigma coordinates at the lowest model levels and the model surface (Simmons et al., 2007). Pressure in the eta coordinate system is a function of surface pressure (p_s) and a pair of time-independent spatially invariant coefficients denoted by a and b (Eq. (1)) that vary in vertical, but not horizontal dimensions.

$$p_k(\lambda, \varphi, t) = a_k + b_k p_s(\lambda, \varphi, t) \quad (1)$$

here k is a generalized vertical index for each of the 60 vertical model levels, λ represents longitude, φ represents latitude, t represents time, and p_s represents surface pressure. Only the lowest 30 model levels were considered given greater vertical resolution, uncertainties regarding stratosphere-troposphere transport (Sklerak et al., 2014), and the lack of moisture above the 30th model level (Dessler et al., 2014). Assuming a standard surface pressure of 1×10^5 Pa the 30th model level is at 0.2×10^5 hPa such that the lowest 30 model levels approximate the tropospheric depth. The most accurate vertical averages are calculated on original model levels using mass-weighted vertical averages (Trenberth, 1991) denoted by $\langle \cdot \rangle$ in Eq. (2).

$$\langle \cdot \rangle = \int_{p_s}^{ml_{30}} (\cdot) \frac{dp}{g} \quad (2)$$

here ml_{30} represents the 30th model level, p_s represents surface pressure, dp represents the pressure thickness between model layers, and g represents gravitational constant. The mass-weighted vertically averaged horizontal sensible and latent heat fluxes are $\langle vT \rangle$ and $\langle vq \rangle$ respectively where $\mathbf{v} = (u, v)$.

2.3. Data analysis, scaling, and symmetry

Data analyses were performed in three phases and results of the third phase are the focus of this article. First, horizontal heat fluxes that maintain climate equilibrium were quantified over a long period record (1979–2016), averaged vertically, and then scaled. Second, to better understand the influence of Earth's dominant mode of interannual climate variability anomalous heat fluxes were quantified during each ENSO event in the period of record and composite analyses were created based on ENSO event magnitude. Third, the symmetric and asymmetric components of anomalous horizontal sensible and latent heat fluxes were quantified for each composite analysis.

Six-hourly output of each variable (q , T , u , v ; Section 2.2) was multiplied at each grid point to quantify horizontal sensible and latent heat fluxes on each model level. The mass-weighted vertical average was performed at each grid point and results were averaged at monthly intervals for storage in multi-dimensional arrays according to the following structure [latitude, longitude, month of year, year]. NDJ months associated with ENSO events summarized in Table 1 were selected for total, strong, and weak composite analyses. Composite analyses for El Niño and La Niña events of various magnitudes were either added or subtracted from each other to quantify symmetric and asymmetric components, respectively (Zhang et al., 2014). After all aforementioned calculations were made results were scaled to provide horizontal fluxes of sensible and latent heat in the same units ($\text{kJ m}^{-1} \text{s}^{-1}$) to allow for direct comparison (Shaw and Pauluis, 2012). Horizontal fluxes of sensible heat were scaled by the specific heat of water ($4.181 \text{ kJ kg}^{-1} \text{K}^{-1}$) under standard atmospheric conditions (20°C , 101.325 kPa). Horizontal fluxes of latent heat were scaled by the latent heat of vaporization (2265 kJ kg^{-1}) at the same standard atmospheric conditions. Additionally, vectors on each plot were scaled to the

maximum value of each color bar to clarify spatial patterns between anomalous maxima of horizontal heat fluxes. This scaling procedure did not change vector trajectories.

The symmetric component of anomalous horizontal, tropospheric-mean fluxes of sensible and latent heat was quantified by subtracting composite analyses of each vector component during La Niña from that of El Niño composites (Zhang et al., 2014). The asymmetric component of anomalous horizontal, tropospheric-mean fluxes of sensible and latent heat was quantified by adding each vector component of composite analyses of El Niño and La Niña (Zhang et al., 2014). Addition or subtraction of composite analyses was performed after all spatial and temporal averages were performed as described above. Therefore, the symmetric component shows the linearity (i.e. mirror image) of anomalies during El Niño and La Niña events whereas the asymmetric component shows the non-linearity (i.e. El Niño is \geq or \leq La Niña) of anomalies. Assuming perfect symmetry, the asymmetric component is equal to zero and symmetric component is double the anomalies associated with either El Niño or La Niña. The symmetric component of anomalous sensible heat fluxes (ASHFs) were used to identify north-south dipoles (NSDs) of anomalous mid-latitude circulations consistent with leading patterns of Northern Hemisphere climate variability (e.g. NAO and PNA). The asymmetric component was used to identify differences in position or intensity of ASHFs associated with NAO or PNA patterns. The symmetric component of anomalous latent heat fluxes

(ALHFs) were used to identify connections between PNA and NAO regions with respective tropical heat source regions. The asymmetric component of ALHFs was used to identify differences in position or magnitude of connections between tropical heat sources and either PNA or NAO regions.

3. Results

3.1. Symmetry of anomalous heat fluxes during all ENSO events

Symmetric and asymmetric components of anomalous sensible heat fluxes (ASHF) during each month of the NDJ period composited over all ENSO events (Table 1) are shown in Fig. 1. While each component of ASHF was of the same order of magnitude ($10^4 \text{ kJ m}^{-1} \text{ s}^{-1}$); maximum anomalies for the symmetric component were larger. Results during November showed a maximum symmetric ASHF of approximately $7 \times 10^4 \text{ kJ m}^{-1} \text{ s}^{-1}$ and a maximum asymmetric ASHF of approximately $2 \times 10^4 \text{ kJ m}^{-1} \text{ s}^{-1}$ across the North Atlantic Ocean. Maxima of the symmetric component of ASHF decreased to approximately $4 \times 10^4 \text{ kJ m}^{-1} \text{ s}^{-1}$ and the asymmetric component increased to approximately $3 \times 10^4 \text{ kJ m}^{-1} \text{ s}^{-1}$ during January. The configuration of the symmetric component of ASHF vectors were used to show north-south dipoles (NSD) consistent with PNA or NAO patterns whereas the asymmetric component showed whether ASHF vectors were larger or

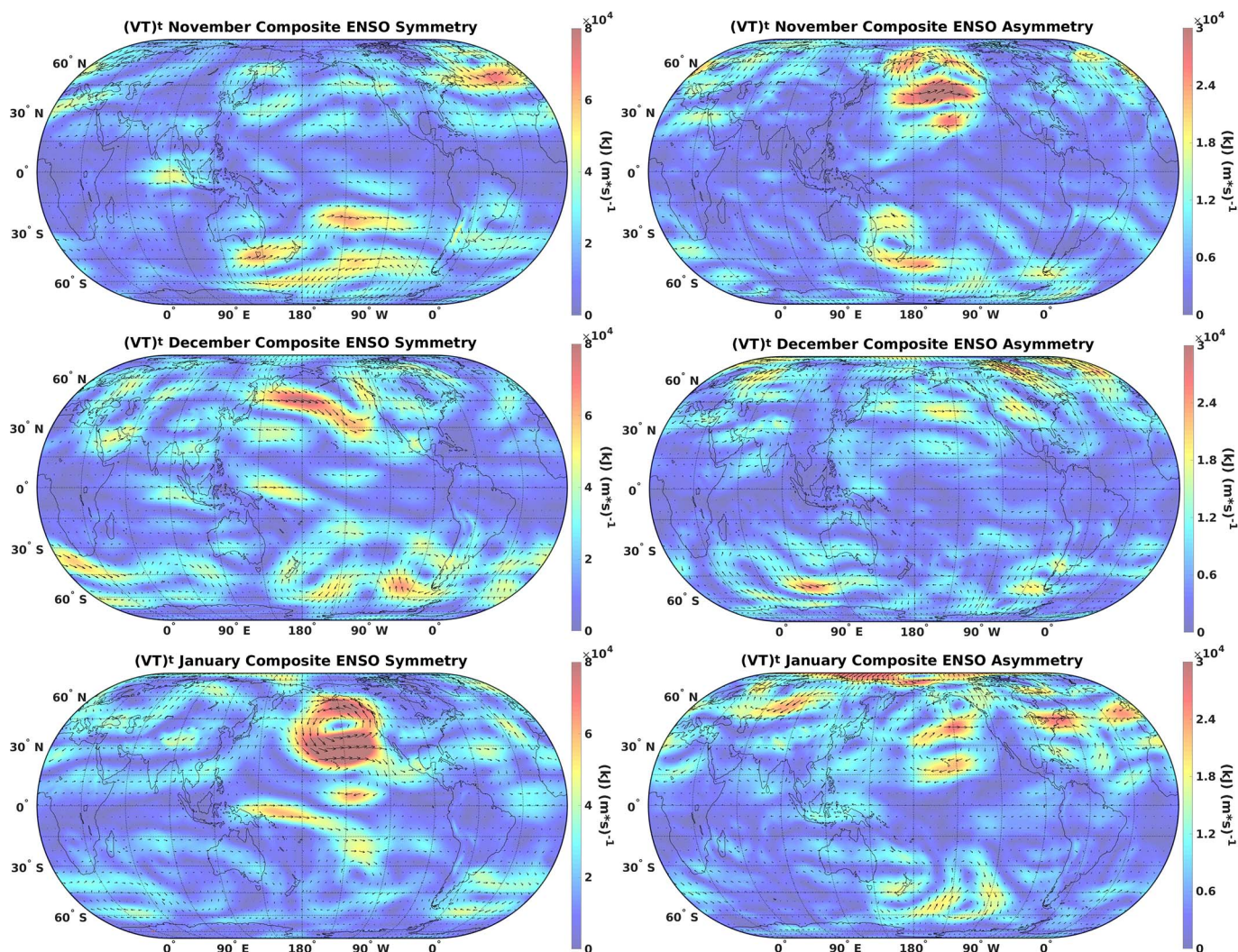


Fig. 1. Symmetric (left) and asymmetric (right) components of monthly (NDJ) tropospheric-mean sensible heat flux anomalies during composites of all El Niño and La Niña events (Table 1) occurring between 1979 and 2016. Color shading represents vector magnitude ($\text{kJ m}^{-1} \text{ s}^{-1}$). (For interpretation of the references to color in this figure legend, the reader is referred to the web version of this article.)

smaller during El Niño or La Niña events. For example, the “November Composite ENSO Symmetry” plot shows a NSD across the North Atlantic Ocean consistent with a positive NAO pattern (Fig. 1). This suggests a linear relationship between ENSO and NAO patterns existed during ENSO events occurring in November. The corresponding asymmetric component shows an east-west circulation dipole (EWD) across the North Atlantic Ocean consistent with a longitudinal shift in the NSD position dependent on phase of ENSO. The configuration of this EWD indicates the positive phase of NAO associated with El Niño is centered nearer the west coast of Europe whereas the negative phase of NAO associated with La Niña is centered nearer the east coast of North America. Therefore, tropospheric mean ASHF’s can provide useful information regarding sub-seasonal patterns of regional symmetry, positioning of NSDs across the North Atlantic Ocean associated with phases of the NAO pattern.

Across the North Pacific Ocean, the symmetric component magnitude of ASHF’s increased each month during the NDJ period and NSDs were apparent for both components of ASHF’s. Results indicate the maximum symmetric component magnitude within the PNA region increased from approximately $4 \times 10^4 \text{ kJ m}^{-1} \text{ s}^{-1}$ during November to $> 8 \times 10^4 \text{ kJ m}^{-1} \text{ s}^{-1}$ during January. Furthermore, a pair of simultaneously out of phase NSDs became apparent across the Northeast Pacific Ocean and North America during December and January consistent with the positive phase of the PNA pattern. This suggests a linear relationship between ENSO and PNA patterns that changes on sub-

seasonal time scales and is particularly apparent during January. The asymmetric component of ASHF’s showed a NSD centered between 140°W and 160°W throughout the NDJ period. Maximum ASHF’s were between $2 \times 10^4 \text{ kJ m}^{-1} \text{ s}^{-1}$ and $3 \times 10^4 \text{ kJ m}^{-1} \text{ s}^{-1}$ during December and January, but were $> 3 \times 10^4 \text{ kJ m}^{-1} \text{ s}^{-1}$ during November. During November, the maximum magnitude of symmetric and asymmetric components of ASHF vectors were similarly large ($\sim 4 \times 10^4 \text{ kJ m}^{-1} \text{ s}^{-1}$) across the northeast Pacific Ocean, but both components were approximately 180° out of phase. Thus, anomalies across the North Atlantic Ocean were approximately 100% larger during La Niña than El Niño across the PNA region during November. During December and January, symmetric and asymmetric components of ASHF vectors were roughly parallel, which is consistent with a linear relationship between ENSO and PNA patterns. However, vector magnitudes of each component indicated a non-linearity in ASHF magnitude across the northeast Pacific Ocean consistent with ASHF’s approximately 25% larger during El Niño rather than La Niña. Therefore, tropospheric mean ASHF’s showed a sub-seasonal dependence to the linear relationship between ENSO and PNA patterns and sub-seasonal differences in the atmospheric response magnitude to each phase of ENSO.

During the boreal winter tropospheric moisture content is small over high latitude continents, including North America, relative to that over ocean basins. Thus, analyses of anomalous latent heat fluxes (ALHF; Fig. 2) were used to clarify low latitude flux patterns and

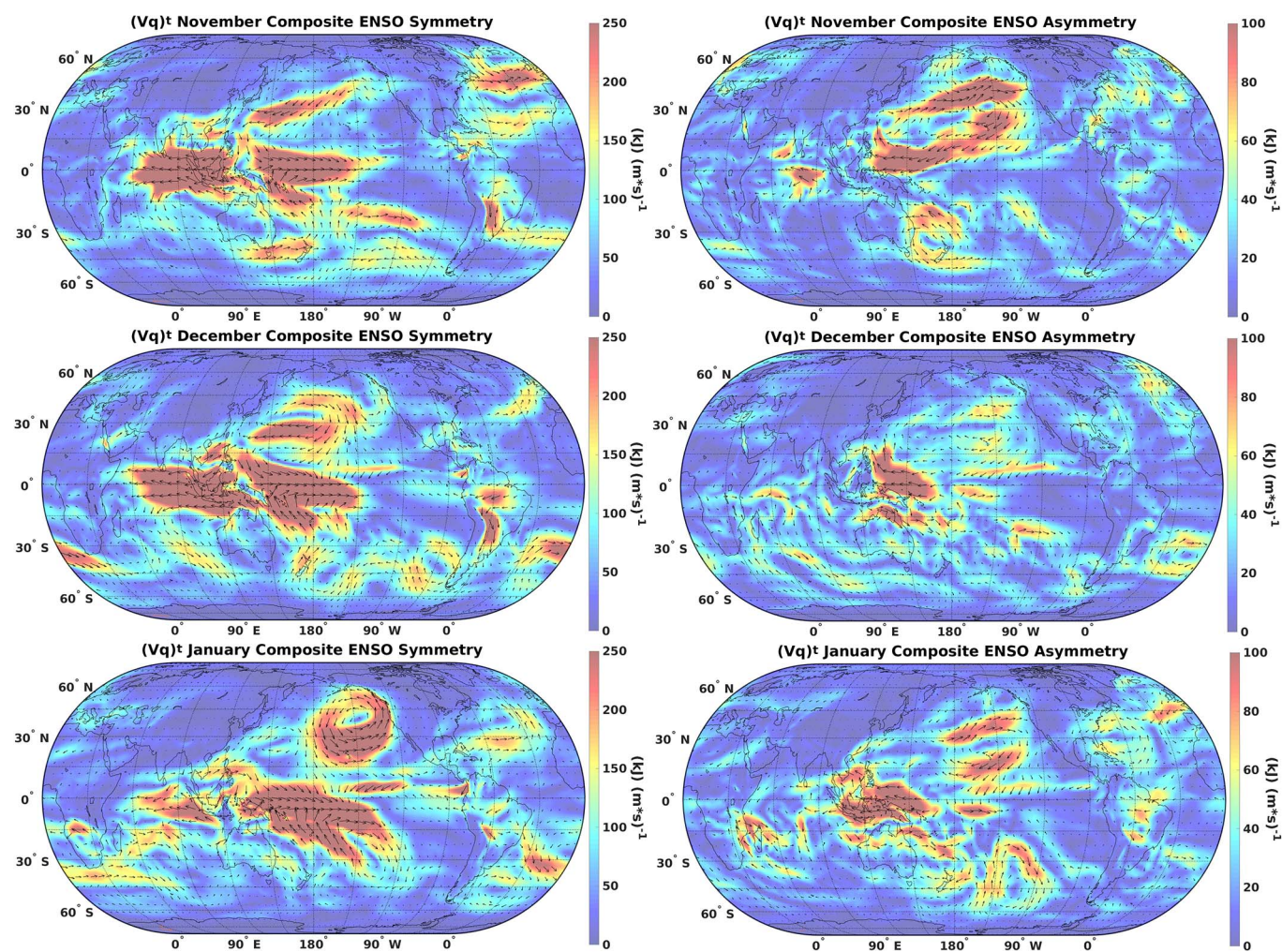


Fig. 2. Symmetric (left) and asymmetric (right) components of monthly (NDJ) tropospheric-mean latent heat flux anomalies during composites of all El Niño and La Niña events (Table 1) occurring between 1979 and 2016. Color shading represents vector magnitude ($\text{kJ m}^{-1} \text{ s}^{-1}$). (For interpretation of the references to color in this figure legend, the reader is referred to the web version of this article.)

identify tropical moisture source regions and their connection to PNA and NAO regions. Across the western equatorial Pacific Ocean, the symmetric component showed a divergent pattern in ALHF vectors during November ($\sim 135^\circ\text{E}$) that shifted west ($\sim 120^\circ\text{E}$) and became less apparent by January. The symmetric component indicated anomalous equatorward fluxes across the entire North Pacific Ocean except along the east coast of Asia and the west coast of North America throughout the NDJ period. This indicates that El Niño events increase poleward fluxes of latent heat along coastal portions of the North Pacific Ocean whereas La Niña events increase poleward fluxes of latent heat across the majority of the ocean basin. The symmetric component of ALHFs indicated a source of anomalous moisture fluxes into the North Atlantic Ocean region transitioned from the subtropical North Atlantic Ocean in November to the Caribbean region in January. Two filaments of ALHFs ($> 100 \text{ kJ m}^{-1} \text{ s}^{-1}$) extended to tropical latitudes suggesting a symmetric connection between the NAO region and both the eastern equatorial Pacific Ocean and equatorial portions of Brazil, particularly during January. This transition can be seen across the Caribbean Sea as anomaly vectors veer (back) from easterly (westerly) in November to southwesterly (northeasterly) in January of El Niño (La Niña) events. The asymmetric component of ALHFs generally revealed similar spatial patterns to that of ASHFs, but provided more detail at low latitudes. Therefore, results in Fig. 2 clarified flux patterns across Pacific and Atlantic Ocean basins, particularly at low latitudes, revealing the sub-

seasonal influence of ENSO phase on tropical moisture sources and their connection to PNA and NAO patterns.

3.2. Symmetry of anomalous heat fluxes during strong ENSO forcing

Symmetric and asymmetric components of ASHF composited over the NDJ period of six strong ENSO events (Table 1) were shown in Fig. 3. Across the North Atlantic Ocean, the symmetric component showed a NSD centered near 30°W consistent with a positive NAO pattern during November and December before shifting east to near the prime meridian during January. This suggests a linear relationship between ENSO and NAO patterns during November and December of strong ENSO events. Across the North Atlantic Ocean, maximum asymmetric component magnitudes of ASHFs increased from approximately $3 \times 10^4 \text{ kJ m}^{-1} \text{ s}^{-1}$ during November to approximately $8 \times 10^4 \text{ kJ m}^{-1} \text{ s}^{-1}$ during January. Increasing ASHF magnitude suggests the relationship between ENSO and NAO patterns became increasingly non-linear throughout the NDJ period. During December and January, the asymmetric component was approximately 180° out of phase with the symmetric component across the North Atlantic Ocean indicating larger anomalies during strong La Niña rather than El Niño events. Across the North Pacific Ocean, the symmetric component of ASHF showed a single NSD during November that became a pair of simultaneously out of phase NSDs consistent with a positive PNA

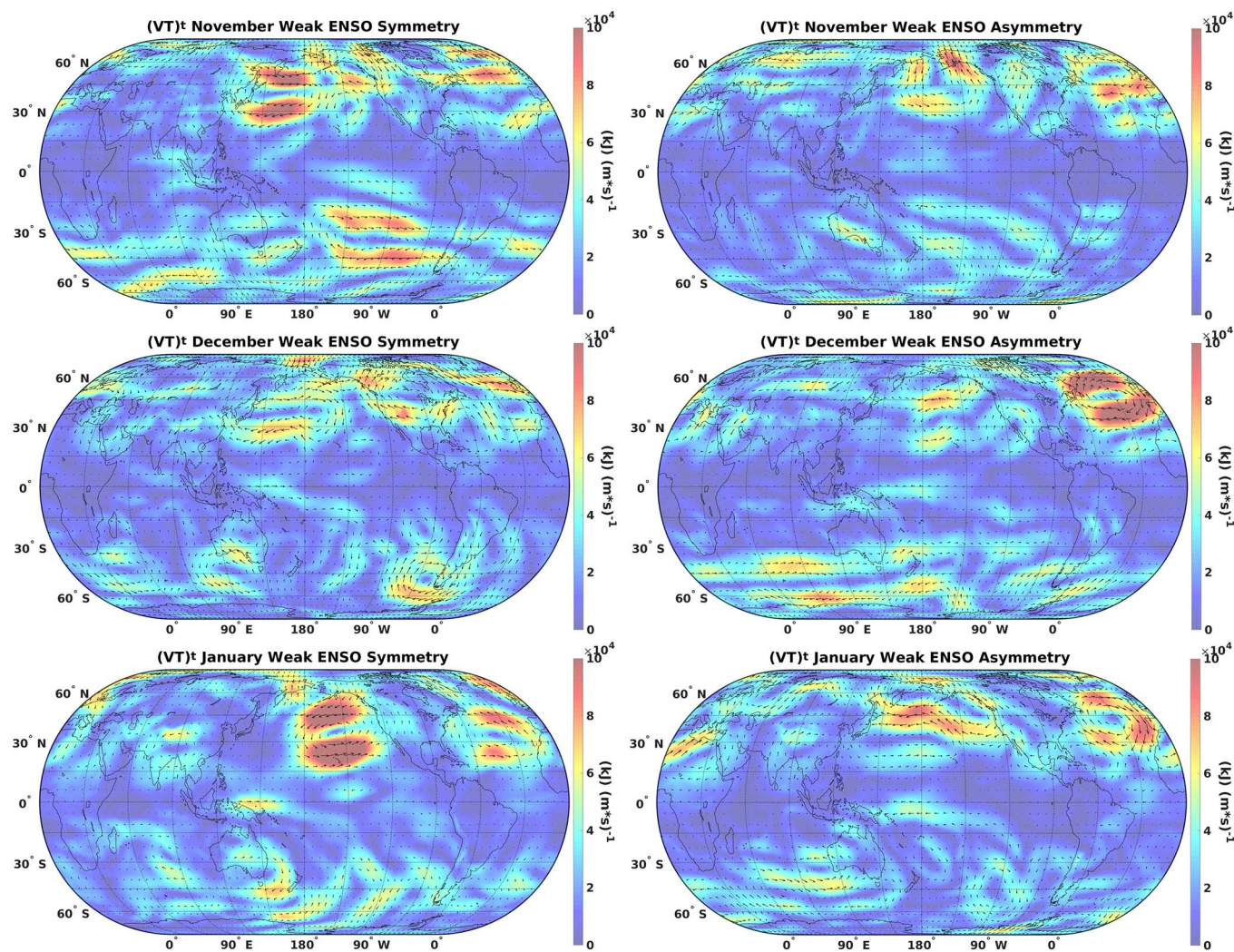


Fig. 3. Symmetric (left) and asymmetric (right) components of monthly (NDJ) tropospheric-mean sensible heat flux anomalies during composites of three strong El Niño (1982–83, 1997–98, and 2015–16) and La Niña (1988–89, 1999–2000, and 2010–11) events occurring between 1979 and 2016. Color shading represents vector magnitude ($\text{kJ m}^{-1} \text{ s}^{-1}$). (For interpretation of the references to color in this figure legend, the reader is referred to the web version of this article.)

pattern during January. The NSD orientation suggests a linear relationship between strong ENSO events and simultaneous PNA patterns similar to Fig. 1, but the asymmetric component showed important positional differences. For strong ENSO events, NSDs apparent in asymmetric component analyses were positioned northeast of corresponding features in Fig. 1, closer to the west coast of North America, throughout the NDJ period. During NDJ asymmetric ASHF vectors were generally oriented in the same direction, but circulation features were positioned northeast of their associated circulations in symmetric component analyses. Differences between symmetric and asymmetric components suggests the NSD across the northeast Pacific Ocean was located nearer the west coast of North America during strong El Niño events whereas it was located farther from the coast during strong La Niña events. Additionally, results show maximum ASHFs were approximately 40% larger along the Pacific Northwest Coast (35° to 50°N) of North America during January of strong El Niño events compared to strong La Niña events. Therefore, a linear relationship between strong ENSO events and both PNA and NAO patterns was apparent and shifts in NSD position across the PNA region were identified dependent on the phase of strong ENSO events.

Symmetric and asymmetric components of ALHF are shown in Fig. 4 and were composited over the NDJ period of six strong ENSO events (Table 1). The symmetric component of ALHFs showed a single NSD centered near 15°W throughout the NDJ period of strong ENSO events resulted in large ALHFs ($> 400 \text{ kJ m}^{-1} \text{ s}^{-1}$) along the west coast of

Europe. Results showed that ALHFs were southwesterly during strong El Niño and northeasterly ALHFs during strong La Niña. The asymmetric component increased across the North Atlantic Ocean during the NDJ period, similar to results shown in Fig. 2. During January the vector components were generally 180° out of phase indicating ALHFs along the west coast of Europe were approximately 50% larger during strong El Niño compared to strong La Niña events. Monthly analyses showed sub-seasonal detail of a connection between equatorial portions of the American continent and southeastern North America, especially the northern Gulf of Mexico coast during December that was symmetric according to phase of strong ENSO events. By January an anomalous cyclonic circulation was centered in the Gulf of Mexico that connected the tropical eastern Pacific Ocean and the east coast of the United States. During December and January, the asymmetric and symmetric vector components were generally parallel in the Gulf of Mexico and Caribbean basins consistent with ALHFs approximately 30% larger during strong El Niño compared to La Niña events. Backing (SW to E) of ALHF vectors across eastern North America throughout the NDJ period appears to be associated with the monthly evolution of the relationship between ENSO and PNA patterns described in the preceding paragraph. Across coastal portions of the North Pacific Ocean poleward ALHF vectors were apparent across extreme southeastern Asia throughout NDJ, which connected with the northwest coast of North America during January. The asymmetric component of ALHF vectors across the North Pacific Ocean generally indicated an EWD, suggesting the NSD

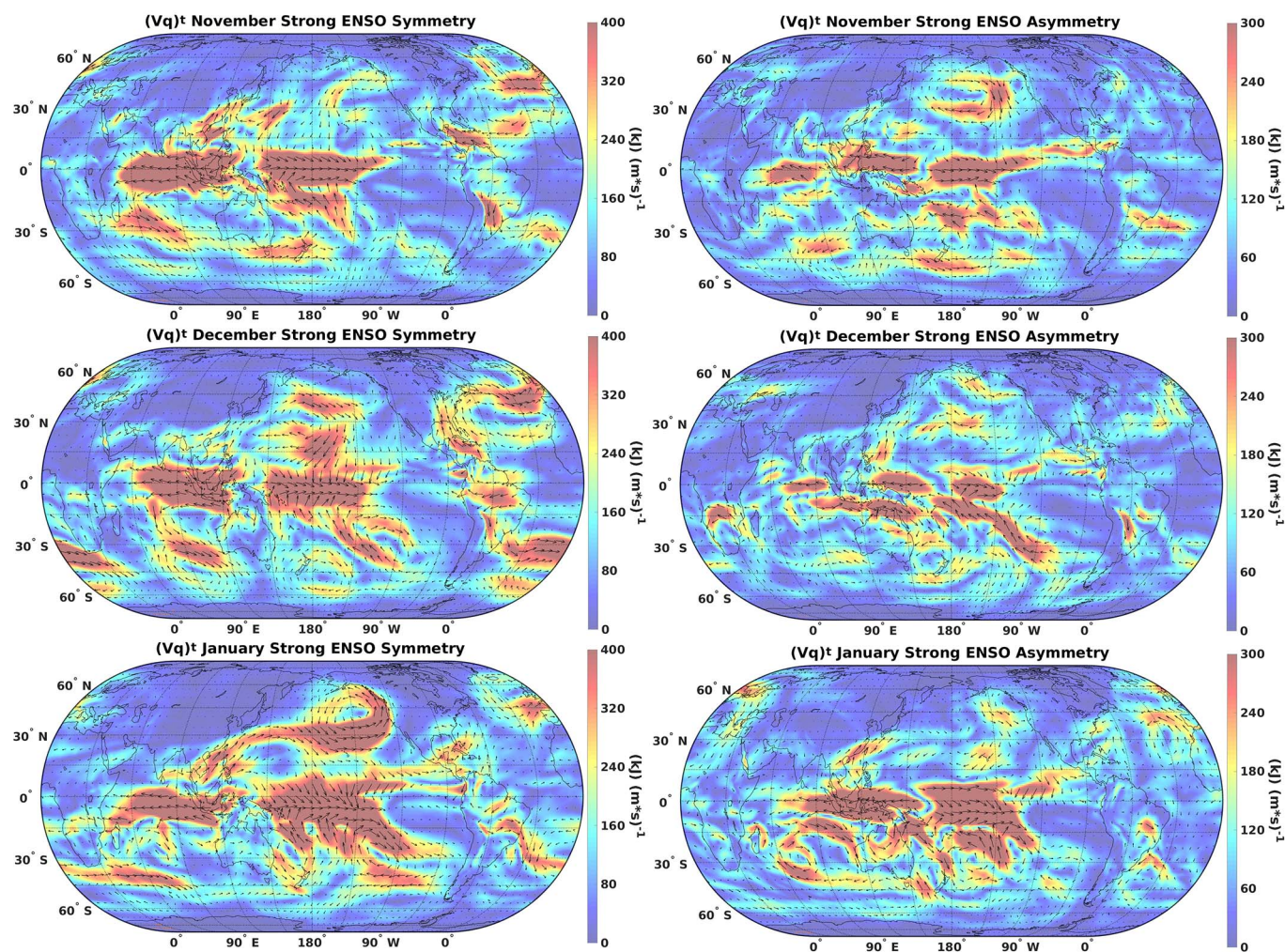


Fig. 4. Symmetric (left) and asymmetric (right) components of monthly (NDJ) tropospheric-mean latent heat flux anomalies during composites of six strong El Niño (1982–83, 1997–98, and 2015–16) and La Niña (1988–89, 1999–2000, and 2010–11) events occurring between 1979 and 2016. Color shading represents vector magnitude ($\text{kJ m}^{-1} \text{ s}^{-1}$). (For interpretation of the references to color in this figure legend, the reader is referred to the web version of this article.)

was closer to (farther from) the west coast of North America during strong El Niño (La Niña) events. Therefore, components of ALHF showed climatologically relevant differences in NSD location and ALHF magnitude for Western Europe and North America during strong ENSO events at sub-seasonal scale.

3.3. Symmetry of anomalous heat fluxes during weak ENSO

The symmetric and asymmetric components of anomalous sensible heat fluxes (ASHFs) composited over six weak ENSO events (Table 1) are shown in Fig. 5. Generally speaking, both components of ASHF are of similar magnitude indicating large differences between each phase of six weak ENSO events. However, each component of ASHFs showed an NSD positioned in the North Atlantic Ocean throughout the NDJ period. The symmetric component showed an NSD consistent with a linear relationship between ENSO and NAO patterns during November and December, which transitioned to a negative linear relationship during January. The negative linear relationship was determined due to larger anomalous heat fluxes at high latitude portions of the North Atlantic Ocean consistent with a NSD. The asymmetric component across the NAO region showed ASHF vectors roughly 180° out of phase with the symmetric component during November and roughly parallel during December and January. Across the North Pacific Ocean, a pair of

simultaneously out of phase NSDs was shown approximately, but did not shift eastwards into the PNA region during December or January. The asymmetric component during November indicated a large anomalous cyclonic circulation centered near 50°N 165°W resulting in generally perpendicular components of ASHF vectors across the North Pacific Ocean. An anomalous cyclonic circulation was apparent in the northeast Pacific Ocean during January, similar to Figs. 1 and 3, but the center of circulation was located approximately 10° southwest of that shown in Fig. 1. The asymmetric component of ASHF vectors were generally 180° out of phase indicating larger ASHFs during December and January of weak La Niña events and important asymmetric positional differences. The asymmetric positional differences suggested that NSDs associated with weak El Niño (La Niña) events were farther from (closer to) the west coast of North America. Therefore, results presented in Fig. 5 showed sub-seasonal details regarding regional patterns associated with weak ENSO events and during Januarys of weak La Niña events generally larger ASHFs positioned nearer the west coast of North America were shown.

Symmetric and asymmetric components of ALHFs associated with weak ENSO events during NDJ are shown in Fig. 6 to provide more detail across ocean basins, particularly at low latitudes. The symmetric component of ALHFs showed a connection between the tropical East Pacific Ocean and North Atlantic Ocean during November of weak La

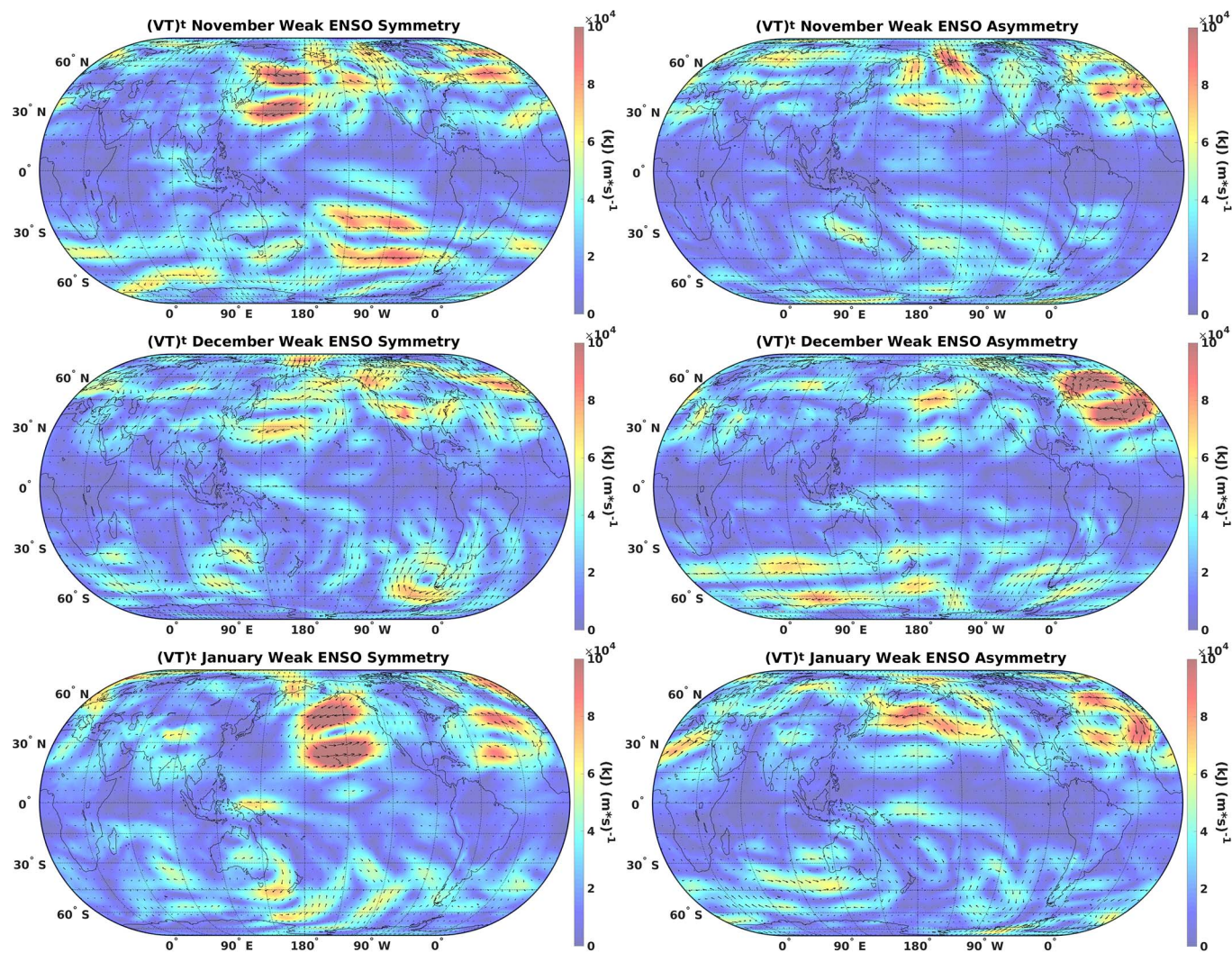


Fig. 5. Symmetric (left) and asymmetric (right) components of monthly (NDJ) tropospheric-mean sensible heat flux anomalies during composite of three weak El Niño (1979–80, 2004–05, and 2014–15) and La Niña (1983–84, 2005–06, and 2008–09) events occurring between 1979 and 2016. Color shading represents vector magnitude ($\text{kJ m}^{-1} \text{s}^{-1}$). (For interpretation of the references to color in this figure legend, the reader is referred to the web version of this article.)

Niña events. During December and January, results indicated a transition from a positive to a negative linear relationship between weak ENSO events and NAO patterns. The asymmetric component indicated that the tropical East Pacific Ocean may be an additional source (sink) for larger (smaller) ALHFs across the North Atlantic Ocean during weak La Niña (El Niño) events. Across the North Pacific Ocean, the symmetric component of ALHFs indicates a spatially continuous connection between the west coast of North America and the tropical West Pacific warm pool during November and December of weak La Niña events. Furthermore, the asymmetric component indicates larger ALHFs during weak La Niña events throughout the NDJ period, particularly along the west coast of North America where the symmetric component indicates anomalous onshore latent heat fluxes. Also of note is the equatorial Pacific Ocean where asymmetric component vectors have similar magnitudes to the symmetric component, but have different areas and vector component headings. This indicates weak La Niña events influence tropospheric latent heat anomalies over a larger tropical area than weak El Niño events, which could explain why asymmetric and symmetric components of ASHF and ALHFs were generally 180° out of phase across the North Pacific Ocean. Therefore, results shown in Fig. 6 indicated larger ALHFs during weak La Niña rather than El Niño events and it is hypothesized that weak La Niña events have connections to broader tropical heat sources than weak El Niño events.

4. Discussion

Earth's horizontal tropospheric circulation is influenced, on a quasi-regular basis, by anomalous vertical heat fluxes from the equatorial Pacific Ocean commonly referred to as ENSO (Peixoto and Oort, 1992). Anomalous vertical heat fluxes into the tropical atmosphere are not of a symmetric magnitude or duration (e.g. An and Jin, 2004; Okumura and Deser, 2010), but must be transported poleward to maintain climate equilibrium (e.g. Kim and Alexander, 2015). Furthermore, poleward transports associated with ENSO have been found to project onto North Atlantic Oscillation (NAO) and Pacific North American (PNA) patterns of intra-annual climate variability (e.g. Liu and Alexander, 2007; Hurrell and Deser, 2010). However, a limited number of studies have directly quantified horizontal heat flux anomalies in the troposphere, their symmetry, or sub-seasonal interrelationships during ENSO events as was shown in this work (e.g. Kim and Alexander, 2015).

4.1. North Atlantic Oscillation

The symmetric component of anomalous sensible and latent heat fluxes was composited over six strong, six weak, and all 25 ENSO events in the period of record (1979–2016). Results showed the sub-seasonal temporal evolution of north to south oriented dipoles (NSDs) across the North Atlantic and North Pacific Oceans. NSDs positioned near

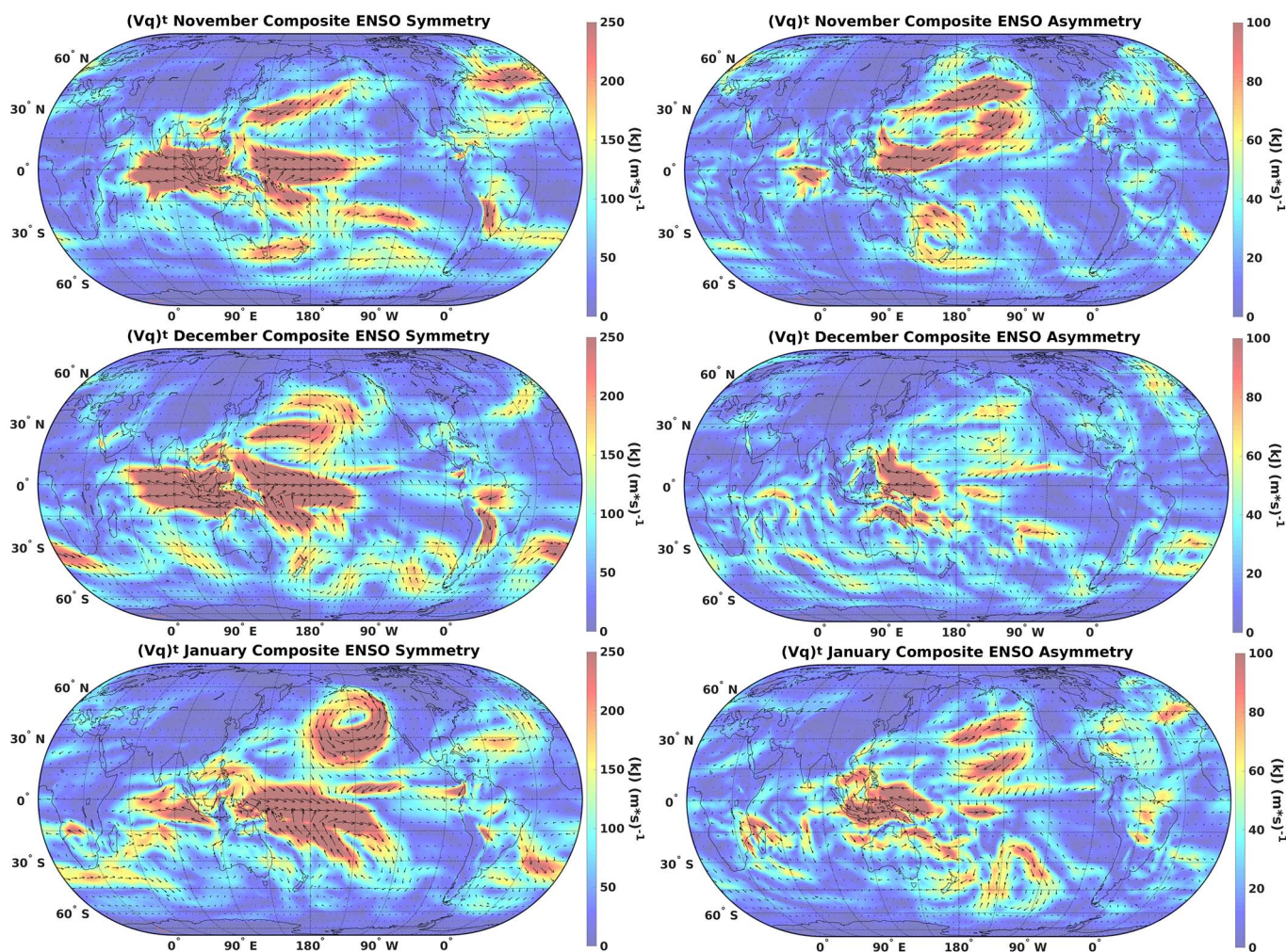


Fig. 6. Symmetric (left) and asymmetric (right) components of monthly (NDJ) tropospheric-mean latent heat flux anomalies during composite of three weak El Niño (1979–80, 2004–05, and 2014–15) and La Niña (1983–84, 2005–06, and 2008–09) events occurring between 1979 and 2016. Color shading represents vector magnitude ($\text{kJ m}^{-1} \text{s}^{-1}$). (For interpretation of the references to color in this figure legend, the reader is referred to the web version of this article.)

Table 2
Summary of implied linear relationships between ENSO events of various magnitude and NAO or PNA patterns of regional climate variability.

		Nov	Dec	Jan
All 25	NAO	+	X	X
	PNA	X	+	+
6 Strong	NAO	+	+	+
	PNA	X	+	+
6 Weak	NAO	+	+	–
	PNA	X	X	X

+ = positive linear, – = negative linear, X = undetermined.

representative locations for PNA (45°N 165°W) and NAO (65°N 30°W) patterns (Hurrell and Deser, 2010) in the symmetric component of ASHF's subjectively implied linear relationships to ENSO events of variable magnitude that were summarized in Table 2. Hurrell and Deser (2010) concluded that no universally accepted index to describe the temporal evolution of the NAO pattern existed, which is why spatial patterns of NSDs were acceptable for this study. All composite analyses indicated a positive linear relationship between ENSO and NAO patterns during November consistent with Huang et al. (1998). However, the signal in late fall and early winter has been shown to be different, and in some cases opposite, from the late winter signal (e.g. Mariotti et al., 2005; Knippertz et al., 2003). Figs. 1, 2, 5, and 6 showed a symmetric anomalous cyclonic circulation centered near 45°W 40°N during January that may represent the onset of a late winter negative linear relationship consistent with results from Brönnimann (2007) and Ineson and Scaife (2009). Additionally, composite analyses based on ENSO event magnitude implied a faster (slower) transition during weak (strong) ENSO events. Brönnimann (2007) discusses this transition as a complicating factor when comparing different studies such that a mixed signal should be expected with traditional composite analyses over the winter season (December–January). Therefore, a transition from a positive to negative linear relationship between ENSO forcing and NAO patterns was apparent, which occurred over sub-seasonal time scales such that future studies should analyze the relationship at sub-seasonal time scales.

The implied transition from a positive to negative linear relationship during the late fall to late winter months is consistent with the increasingly popular notion that inter-event variability of ENSO effects in Europe is systematic (Brönnimann, 2007). Brönnimann (2007) further explained that the signal leaving the tropical Pacific Ocean varies for each ENSO event, but it may be modulated or modified in a systematic manner. Results presented in this work imply anomalous heat fluxes between Atlantic and Pacific Ocean basins may be a systematic factor influencing the relationship between ENSO and NAO patterns, which may not have been discussed in existing literature. Figs. 1 and 2 showed anomalous heat fluxes across Central America from the Pacific Ocean into the Atlantic Ocean basin during El Niño events that increased in magnitude throughout the NDJ period. Furthermore, strong El Niño (La Niña) events (Figs. 3 and 4) resulted in anomalous heat fluxes into (out of) the Atlantic Ocean basin at least 100% larger than Figs. 1 or 2 whereas weak ENSO events (Figs. 5 and 6) did not show a connection between ocean basins. Anomalous latent heat fluxes (ALHF's) clarified low latitude patterns and showed veering (backing) across the West Atlantic Ocean throughout the NDJ period (Fig. 2) consistent with increasing (decreasing) Pacific Ocean influence during El Niño (La Niña) events. Therefore, the influx of sensible and latent heat from the Pacific Ocean could be a modulating factor for the relationship between ENSO and NAO that is systematically symmetric about both ENSO phases and increases with ENSO event magnitude.

Toniazzo and Scaife (2006) concluded that the effects of El Niño events increase with El Niño event magnitude and those effects were highly non-linear during January and February across the NAO region. Results during January indicated that the direction of circulation

reversed depending on ENSO magnitude, which was consistent with results of Toniazzo and Scaife (2006). Multiple asymmetries in anomalous heat flux magnitude and NSD position were also identified across a spectrum of ENSO event magnitudes confirming that linear methods such as correlation are insufficient to resolve all mid-latitude effects from ENSO events (Brönnimann, 2007). Figs. 1 through 4 showed maximum vector magnitudes of symmetric and asymmetric components converge to similar values across the North Atlantic Ocean implying increasing non-linearity throughout NDJ. Vector component magnitudes were not found to converge in composites of weak ENSO events, which were shown to be strongly asymmetric throughout the NDJ period. Large asymmetry during weak ENSO events and increasing asymmetry throughout NDJ of other composite analyses could be a key factor limiting correlation analyses (e.g. Rocha, 1999; Wang, 2002) and preventing agreement with alternative methods (i.e. compositing). In particular, Fig. 1 indicated larger anomalous heat fluxes near the west coast of Europe during November of El Niño events, which transitioned to the east coast of North America by January of El Niño and vice versa for La Niña events. These spatial patterns and other examples of asymmetry in positioning of NSDs, magnitude of anomalous heat fluxes associated with these NSDs, and magnitude of ENSO events cannot be identified through correlation analyses. Therefore, composite analyses of anomalous tropospheric-mean heat fluxes could be a valuable addition to existing statistical methods for assessing a relationship between ENSO and NAO patterns of climate variability.

4.2. Pacific North American pattern

Understanding of the influence ENSO has on extra-tropical climate across the Pacific basin and North American continent is better than that across the North Atlantic Ocean (Brönnimann, 2007). Straus and Shukla (2002) concluded that the presence of ENSO forcing skewed the probability of positive or negative phases of the PNA pattern such that a positive linear relationship between ENSO and PNA patterns is commonly observed. Results of this work, particularly during December and January, were consistent with a positive linear relationship between ENSO and PNA patterns. Anomalous heat flux asymmetries were shown to be larger across the Northeast Pacific Ocean associated with El Niño as compared to La Niña events, particularly during December and January. Asymmetry in ASHF and ALHF magnitude could be directly attributable to the inherent asymmetry of SSTA magnitudes associated with the ENSO phenomena (Okumura and Deser, 2010) and differences in anomalous heat fluxes may be proportional to asymmetries in SSTA magnitude. Additionally, asymmetries in NSD position were apparent associated with variable ENSO event amplitudes. During January of weak (strong) El Niño events the NSD was located further from (closer to) the west coast of North America and vice versa for La Niña events. These positional differences imply the greatest climate anomalies along the west coast of North America during strong El Niño and weak La Niña events. Given the lack of studies examining the atmospheric response to La Niña events or the symmetry of the response (e.g. Brönnimann, 2007; Okumura and Deser, 2010), this may be the first study to identify climatologically relevant patterns associated with weak La Niña events. The asymmetries found in this work may have been missed without sub-seasonal details provided by monthly analyses, which was uncharacteristic of similar studies. Therefore, results confirmed findings of previous studies while adding sub-seasonal details to the temporal evolution of both symmetric and asymmetric components of the atmospheric response including changes associated with ENSO forcing of variable magnitude.

4.3. Atmospheric rivers

The influence of ENSO on the frequency and magnitude of atmospheric rivers impacting the west coast of North America remains unclear (Gimeno et al., 2014), but previous studies have found

atmospheric rivers to be most frequent during near-neutral ENSO conditions (Bao et al., 2006; Dettinger, 2004). However, results presented in Figs. 3 and 4 showed spatial patterns consistent with Maya and Pineapple express atmospheric river phenomena during strong El Niño events. Across the West Atlantic Ocean, strong El Niño events resulted in large ($> 300 \text{ kJ m}^{-1} \text{ s}^{-1}$) poleward ALHFs connecting both the tropical east Pacific Ocean and Caribbean Sea with eastern United States similar to a Maya Express atmospheric river (Dirmeyer and Kinter, 2010). Across the North Pacific Ocean, large ($> 300 \text{ kJ m}^{-1} \text{ s}^{-1}$) ALHFs connected extreme Southeast Asia and the west coast of North America in a similar manner to the Pineapple Express atmospheric river phenomena (Lackmann and Gyakum, 1999). The connection to extreme Southeast Asia challenges the commonly accepted description of a Pineapple Express event, which indicates a moisture source emanating from the central Pacific Ocean near the Hawaiian Islands (Gimeno et al., 2014). However, results presented in Fig. 6 indicated more direct transport onto the west coast of North America emanating from the Hawaiian Island region that is more consistent with a canonical Pineapple Express event and was favored during weak (i.e. near-neutral) El Niño conditions. Additionally, Fig. 6 indicated a narrow filament of large ALHFs connecting the tropical West Pacific Ocean with the west coast of North America during weak La Niña events. Therefore, ALHF analyses indicated patterns consistent with atmospheric river phenomena across a spectrum of ENSO event magnitudes and provided clarification of the tropical source regions at sub-seasonal time scales.

4.4. Asymmetry of tropospheric anomalies

ENSO is inherently asymmetric for both SSTA magnitude and duration (Okumura and Deser, 2010) and results presented in this work support the notion that that asymmetry is a fundamental property of the atmospheric response to ENSO as well (Zhang et al., 2014). Tropospheric results presented in this work confirmed that both components of anomalous horizontal heat fluxes are of the same order of magnitude implying climatologically relevant impacts associated with each component (Zhang et al., 2014). Furthermore, this work indicated asymmetries in positioning of NSDs, the magnitude of ASHF or ALHF anomalies for each phase of ENSO, and composite analyses of ENSO events stratified by event amplitude. These asymmetries cannot be identified through traditional correlation techniques (Brönnimann, 2007), but can be identified through careful analysis of anomalous horizontal heat fluxes averaged through the approximate tropospheric depth. Therefore, asymmetry is a fundamental property of the atmospheric response to ENSO, which strongly indicates methods separate from correlation analyses are necessary to fully understand global impacts associated with ENSO.

While results showed tropospheric symmetry in the linear relationship between ENSO, PNA, and NAO; substantial intra-seasonal variability existed and multiple other studies have found contrary results (e.g. Pozo-Vázquez et al. 2005a; Pozo-Vázquez et al. 2005b; Quadrelli et al. 2001; Wang, 2002). However, comparisons between studies are limited by differences in statistical methods, ENSO criteria, definitions of seasons, and data used. Additionally, the notion that both ENSO and the atmospheric response to ENSO are strongly asymmetric has complicated efforts to correlate ENSO, PNA, and NAO patterns. Therefore, sub-seasonal pattern identification should be preferred over seasonal analyses given that both PNA and NAO vary on intra-annual time scales.

5. Conclusions

In this study, we quantified symmetric and asymmetric components of anomalous horizontal fluxes of sensible and latent heat during ENSO events using ERA-Interim data. The key findings include the following:

- Interrelationships between ENSO, PNA, and NAO patterns were determined at sub-seasonal time scales (Table 2). Results indicated a transition from positive to negative linear relationship between ENSO and NAO whereas the relationship between ENSO and PNA was consistently positive, but the onset was typically delayed until December.
- Spatially continuous connections between tropical moisture sources and the PNA and NAO regions were identified as well as spatial patterns consistent with atmospheric river phenomena impacting both West and East coasts of North America.
- The influence of ENSO event amplitude was shown to be large and influenced both the interrelationship between ENSO, PNA, and NAO patterns as well as the spatially continuous connections between tropical moisture sources and mid-latitude circulations.

Therefore, analyses of anomalous heat fluxes provided new information regarding the interrelationship between ENSO and both NAO and PNA patterns through sub-seasonal analyses. Additionally, results showed the structure and direction of poleward heat flux anomalies such that ASHF and ALHF analyses should be considered a valuable addition to existing methods to assess climate variability across a broad range of spatiotemporal scales.

Acknowledgements

Appreciation is extended to anonymous external evaluations of the article that greatly improved the quality of the work. This research did not receive any specific grant from funding agencies in the public, commercial, or not-for-profit sectors.

References

- Alexander, M.A., Bladé, I., Newman, M., Lanzante, J.R., Lau, N.C., Scott, J.D., 2002. The atmospheric bridge: the influence of ENSO teleconnections on air–sea interaction over the global oceans. *J. Clim.* 15 (16), 2205–2231 (DOI: [http://dx.doi.org/10.1175/1520-0442\(2002\)015%3C2205:TABTIO%3E2.0.CO;2](http://dx.doi.org/10.1175/1520-0442(2002)015%3C2205:TABTIO%3E2.0.CO;2)).
- An, S.I., Jin, F.F., 2004. Nonlinearity and asymmetry of ENSO. *J. Clim.* 17 (12), 2399–2412 (DOI: [http://dx.doi.org/10.1175/1520-0442\(2004\)017%3C2399:NAAOE%3E2.0.CO;2](http://dx.doi.org/10.1175/1520-0442(2004)017%3C2399:NAAOE%3E2.0.CO;2)).
- Bao, J.W., Michelson, S.A., Neiman, P.J., Ralph, F.M., Wilczak, J.M., 2006. Interpretation of enhanced integrated water vapor bands associated with extratropical cyclones: their formation and connection to tropical moisture. *Mon. Weather Rev.* 134, 1063–1080. <http://dx.doi.org/10.1175/MWR3123.1>.
- Brönnimann, S., 2007. Impact of El Niño–Southern Oscillation on European climate. *Rev. Geophys.* 45 (3). <http://dx.doi.org/10.1029/2006RG000199>.
- Dee, D.P., Uppala, S.M., Simmons, A.J., Berrisford, P., Poli, P., Kobayashi, S., Andrae, U., Balmaseda, M.A., Balsamo, G., Bauer, P., Bechtold, P., 2011. The ERA-interim reanalysis: configuration and performance of the data assimilation system. *Q. J. R. Meteorol. Soc.* 137 (656), 553–597. <http://dx.doi.org/10.1002/qj.828>.
- Dessler, A.E., Schoeberl, M.R., Wang, T., Davis, S.M., Rosenlof, K.H., Vernier, J.P., 2014. Variations of stratospheric water vapor over the past three decades. *J. Geophys. Res. Atmos.* 119 (22). <http://dx.doi.org/10.1002/2014JD021712>.
- Dettinger, M.D., 2004. Fifty-two Years of Pineapple-express Storms Across the West Coast of North America. U.S. Geological Survey, Scripps Institution Of Oceanography For The California Energy Commission, Pier Energy-Related Environmental Research. CEC-500-2005-004.
- Dirmeier, P.A., Kinter III, J.L., 2010. Floods over the US midwest: a regional water cycle perspective. *J. Hydrometeorol.* 11 (5), 1172–1181. <http://dx.doi.org/10.1175/2010JHM1196.1>.
- Fogt, R.L., Bromwich, D.H., 2006. Decadal variability of the ENSO teleconnection to the high-latitude South Pacific governed by coupling with the southern annular mode. *J. Clim.* 19 (6), 979–997. <http://dx.doi.org/10.1175/JCLI3671.1>.
- Franzke, C., Feldstein, S.B., Lee, S., 2011. Synoptic analysis of the Pacific–North American teleconnection pattern. *Q. J. R. Meteorol. Soc.* 137 (655), 329–346. <http://dx.doi.org/10.1002/qj.768>.
- Fu, G., Charles, S.P., Timbal, B., Jovanovic, B., Ouyang, F., 2016. Comparison of NCEP–NCAR and ERA-interim over Australia. *Int. J. Climatol.* <http://dx.doi.org/10.1002/joc.4499>.
- Fu, C., Yao, H., 2015. Trends of ice breakup date in south-central Ontario. *J. Geophys. Res. Atmos.* 120 (18), 9220–9236. <http://dx.doi.org/10.1002/2015JD023370>.
- Gimeno, L., Nieto, R., Vázquez, M., Lavers, D.A., 2014. Atmospheric rivers: a mini-review. *Front. Earth Sci.* 2, 2. <http://dx.doi.org/10.3389/feart.2014.00002>.
- Harrison, D.E., Chioldi, A.M., 2017. Comments on “characterizing ENSO coupled variability and its impact on North American Seasonal precipitation and temperature”. *J. Clim.* 30 (1), 427–436. <http://dx.doi.org/10.1175/JCLI-D-15-0678.1>.
- Huang, J., Higuchi, K., Shabbar, A., 1998. The relationship between the North Atlantic

- oscillation and El Niño-southern oscillation. *Geophys. Res. Lett.* 25, 2707–2710.
- Hurrell, J.W., Deser, C., 2010. North Atlantic climate variability: the role of the North Atlantic oscillation. *J. Mar. Syst.* 79 (3), 231–244. <http://dx.doi.org/10.1016/j.jmarsys.2009.11.002>.
- Ineson, S., Scaife, A.A., 2009. The role of the stratosphere in the European climate response to El Niño. *Nat. Geosci.* 2 (1), 32–36. <http://dx.doi.org/10.1038/ngeo381>.
- Kim, H.M., Alexander, M.A., 2015. ENSO's modulation of water vapor transport over the Pacific-North American region. *J. Clim.* 28 (9), 3846–3856. <http://dx.doi.org/10.1175/JCLI-D-14-00725.1>.
- Kirtman, B.P., Min, D., Infanti, J.M., Kinter III, J.L., Paolino, D.A., Zhang, Q., Van Den Dool, H., Saha, S., Mendez, M.P., Becker, E., Peng, P., 2014. The North American multimodel ensemble: phase-1 seasonal-to-interannual prediction; phase-2 toward developing intraseasonal prediction. *Bull. Am. Meteorol. Soc.* 95 (4), 585–601. <http://dx.doi.org/10.1175/BAMS-D-12-00050.1>.
- Knippertz, P., Ulbrich, U., Marques, F., Corte-Real, J., 2003. Decadal changes in the link between El Niño and springtime North Atlantic oscillation and European-North African rainfall. *Int. J. Climatol.* 23, 1293–1311.
- Lackmann, G.M., Gyakum, J.R., 1999. Heavy cold-season precipitation in the northwestern United States: Synoptic climatology and an analysis of the flood of 17–18 January 1986. *Weather Forecast.* 14 (5), 687–700.
- Lau, N.C., Nath, M.J., 1996. The role of the “atmospheric bridge” in linking tropical Pacific ENSO events to extratropical SST anomalies. *J. Clim.* 9 (9), 2036–2057 (DOI: [http://dx.doi.org/10.1175/1520-0442\(1996\)009%3C2036:TROTBI%3E2.0.CO;2](http://dx.doi.org/10.1175/1520-0442(1996)009%3C2036:TROTBI%3E2.0.CO;2)).
- Leathers, D.J., Palecki, M.A., 1992. The Pacific/North American teleconnection pattern and United States climate. Part II: temporal characteristics and index specification. *J. Clim.* 5 (7), 707–716 (DOI: [http://dx.doi.org/10.1175/1520-0442\(1992\)005%3C0707:TPATPA%3E2.0.CO;2](http://dx.doi.org/10.1175/1520-0442(1992)005%3C0707:TPATPA%3E2.0.CO;2)).
- Leathers, D.J., Yarnal, B., Palecki, M.A., 1991. The Pacific/North American teleconnection pattern and United States climate. Part I: regional temperature and precipitation associations. *J. Clim.* 4 (5), 517–528 (DOI: [http://dx.doi.org/10.1175/1520-0442\(1991\)004%3C0517:TPATPA%3E2.0.CO;2](http://dx.doi.org/10.1175/1520-0442(1991)004%3C0517:TPATPA%3E2.0.CO;2)).
- Liu, Z., Alexander, M., 2007. Atmospheric bridge, oceanic tunnel, and global climatic teleconnections. *Rev. Geophys.* 45 (2). <http://dx.doi.org/10.1029/2005RG000172>.
- Lorenz, C., Kunstmann, H., 2012. The hydrological cycle in three state-of-the-art re-analyses: intercomparison and performance analysis. *J. Hydrometeorol.* 13 (5), 1397–1420. <http://dx.doi.org/10.1175/JHM-D-11-088.1>.
- Mariotti, A., Ballabrera-Poy, J., Zeng, N., 2005. Tropical influence on Euro-Asian autumn rainfall variability. *Clim. Dyn.* 24, 511–521.
- Müller, W.A., Roeckner, E., 2008. ENSO teleconnections in projections of future climate in ECHAM5/MPI-OM. *Clim. Dyn.* 31 (5), 533–549. <http://dx.doi.org/10.1007/s00382-007-0357-3>.
- Okumura, Y.M., Deser, C., 2010. Asymmetry in the duration of El Niño and La Niña. *J. Clim.* 23 (21), 5826–5843. <http://dx.doi.org/10.1175/2010JCLI3592.1>.
- Peixoto, J.P., Oort, A.H., 1992. *Physics of Climate*.
- Pozo-Vázquez, D., Gámiz-Fortis, S.R., Tovar-Pescador, J., Esteban-Parra, M.J., Castro-Díez, Y., 2005a. ENSO events and associated European winter precipitation anomalies. *Int. J. Climatol.* 25, 17–31.
- Pozo-Vázquez, D., Gámiz-Fortis, S.R., Tovar-Pescador, J., Esteban-Parra, M.J., Castro-Díez, Y., 2005b. North Atlantic winter SLP anomalies based on the autumn ENSO state. *J. Clim.* 18, 97–103.
- Quadrelli, R., Pavan, V., Molteni, F., 2001. Wintertime variability of Mediterranean precipitation and its links with large-scale circulation anomalies. *Clim. Dyn.* 17, 457–466.
- Rocha, A., 1999. Low-frequency variability of seasonal rainfall over the Iberian Peninsula and ENSO. *Int. J. Climatol.* 19, 889–901.
- Rodionov, S.N., Bond, N.A., Overland, J.E., 2007. The Aleutian Low, storm tracks, and winter climate variability in the Bering Sea. *Deep-Sea Res. II Top. Stud. Oceanogr.* 54 (23), 2560–2577. <http://dx.doi.org/10.1016/j.dsr2.2007.08.002>.
- Rodwell, M.J., Rowell, D.P., Folland, C.K., 1999. Oceanic forcing of the wintertime North Atlantic oscillation and European climate. *Nature* 398 (6725), 320–323. <http://dx.doi.org/10.1038/18648>.
- Seager, R., Kushnir, Y., Nakamura, J., Ting, M., Naik, N., 2010. Northern hemisphere winter climate variability: ENSO, NAO and the winter of 2009/10. *Geophys. Res. Lett.* 37 (14). <http://dx.doi.org/10.1029/2010GL043830>.
- Serreze, M.C., Carse, F., Barry, R.G., Rogers, J.C., 1997. Icelandic low cyclone activity: climatological features, linkages with the NAO, and relationships with recent changes in the Northern hemisphere circulation. *J. Clim.* 10 (3), 453–464 (DOI: [http://dx.doi.org/10.1175/1520-0442\(1997\)010%3C0453:ILCACF%3E2.0.CO;2](http://dx.doi.org/10.1175/1520-0442(1997)010%3C0453:ILCACF%3E2.0.CO;2)).
- Shaw, T.A., Pauluis, O., 2012. Tropical and subtropical meridional latent heat transports by disturbances to the zonal mean and their role in the general circulation. *J. Atmos. Sci.* 69 (6), 1872–1889. <http://dx.doi.org/10.1175/JAS-D-11-0236.1>.
- Simmons, A., Uppala, S., Dee, D., Kobayashi, S., 2007. ERA-interim: new ECMWF re-analysis products from 1989 onwards. In: *ECMWF Newsletter*. Vol. 110. pp. 25–35.
- Skerlak, B., Sprenger, M., Wernli, H., 2014. A global climatology of stratosphere-troposphere exchange using the ERA-Interim data set from 1979 to 2011. *Atmos. Chem. Phys.* 14 (2), 913. <http://dx.doi.org/10.5194/acp-14-913-2014>.
- Straus, D.M., Shukla, J., 2002. Does ENSO force the PNA? *J. Clim.* 15 (17), 2340–2358 (DOI: [http://dx.doi.org/10.1175/1520-0442\(2002\)015%3C2340:DEFTF%3E2.0.CO;2](http://dx.doi.org/10.1175/1520-0442(2002)015%3C2340:DEFTF%3E2.0.CO;2)).
- Toniazzo, T., Scaife, A.A., 2006. The influence of ENSO on winter North Atlantic climate. *Geophys. Res. Lett.* 33 (24).
- Trenberth, K.E., 1991. Climate diagnostics from global analyses: conservation of mass in ECMWF analyses. *J. Clim.* 4 (7), 707–722 (DOI: [http://dx.doi.org/10.1175/1520-0442\(1991\)004%3C0707:CDGAC%3E2.0.CO;2](http://dx.doi.org/10.1175/1520-0442(1991)004%3C0707:CDGAC%3E2.0.CO;2)).
- Trenberth, K.E., Branstator, G.W., Karoly, D., Kumar, A., Lau, N.C., Ropelewski, C., 1998. Progress during TOGA in understanding and modeling global teleconnections associated with tropical sea surface temperatures. *J. Geophys. Res. Oceans* 103 (C7), 14291–14324. <http://dx.doi.org/10.1029/97JC01444>.
- Trenberth, K.E., Caron, J.M., 2000. The Southern oscillation revisited: sea level pressures, surface temperatures, and precipitation. *J. Clim.* 13 (24), 4358–4365 (DOI: [http://dx.doi.org/10.1175/1520-0442\(2000\)013%3C4358:TSORSL%3E2.0.CO;2](http://dx.doi.org/10.1175/1520-0442(2000)013%3C4358:TSORSL%3E2.0.CO;2)).
- Trenberth, K.E., Stepaniak, D.P., 2003. Seamless poleward atmospheric energy transports and implications for the Hadley circulation. *J. Clim.* 16 (22), 3706–3722 (DOI: [http://dx.doi.org/10.1175/1520-0442\(2003\)016%3C3706:SPAETA%3E2.0.CO;2](http://dx.doi.org/10.1175/1520-0442(2003)016%3C3706:SPAETA%3E2.0.CO;2)).
- Wang, C., 2002. Atlantic climate variability and its associated atmospheric circulation cells. *J. Clim.* 15, 1516–1536.
- Wolter, K., Timlin, M.S., 2011. El Niño/Southern oscillation behaviour since 1871 as diagnosed in an extended multivariate ENSO index (MEI ext). *Int. J. Climatol.* 31 (7), 1074–1087. <http://dx.doi.org/10.1002/joc.2336>.
- Yu, J.Y., Kim, S.T., 2013. Identifying the types of major El Niño events since 1870. *Int. J. Climatol.* 33 (8), 2105–2112. <http://dx.doi.org/10.1002/joc.3575>.
- Zhang, T., Perlwitz, J., Hoerling, M.P., 2014. What is responsible for the strong observed asymmetry in teleconnections between El Niño and La Niña? *Geophys. Res. Lett.* 41 (3), 1019–1025. <http://dx.doi.org/10.1002/2013GL058964>.